Polymer 51 (2010) 3940–3947

Contents lists available at ScienceDirect

Polymer

journal homepage: www.elsevier.com/locate/polymer

Processing, structure and properties of poly(ether ketone) grafted few wall carbon nanotube composite fibers

Rahul Jain [a,1], Young Ho Choi [a], Yaodong Liu [a], Marilyn L. Minus [a,2], Han Gi Chae [a,**], Satish Kumar [a,**], Jong-Beom Baek [a,b,*]

[a] School of Polymer, Textile and Fiber Engineering, Georgia Institute of Technology, Atlanta, GA 30332, USA
[b] Interdisciplinary School of Green Energy/Institute of Advanced Materials & Devices, Ulsan National Institute of Science and Technology, Ulsan, 689-798, South Korea

ARTICLE INFO

Article history:
Received 5 February 2010
Received in revised form
2 June 2010
Accepted 22 June 2010
Available online 1 July 2010

Keywords:
Carbon nanotube
Poly(ether ketone)
Nanocomposite

ABSTRACT

Poly(ether ketone) (PEK) was grafted onto few wall carbon nanotube (FWNT) using *in-situ* polymerization of 4-phenoxybenzoic acid (4-PBA) in poly(phosphoric acid) (PPA), and fibers were processed using dry-jet wet-spinning. The PEK/FWNT weight ratio was in the range of 99/1 to 80/20. The fibers have been characterized for their morphology, structure, mechanical properties, as well as electrical conductivity. The toughness (work of rupture) of the PEK fibers, as measured from the area under the stress–strain curves, was as high as 130 J/g and often exceeded the toughness of the toughest synthetic fibers such as Kevlar™ (~45 J/g) and Zylon™ (~50 J/g) and approached values closer to that of spider silk (~170 J/g). PEK and PEK-g-FWNT fibers exhibit good thermal stability with degradation onset of above 500 °C under nitrogen environment, and possess high char yield (~50% for 5 wt% FWNT containing PEK fiber). PEK-g-FWNT fibers can be processed that exhibit good dimensional stability up to 300 °C (coefficient of thermal expansion $\sim -1.2 \times 10^{-5}$/°C) and the axial electrical conductivity was as high as 240 S/m at 20 wt% FWNT loading.

1. Introduction

Poly(ether ketone) (PEK) is a promising engineering polymer with high thermal stability [1,2]. However, high melting temperature (close to its degradation temperature) and high melt viscosity of PEK limits its processibility. In addition, the typical polymerization route for PEK has not allowed for the production of high molecular weight PEK, and this has also limited its use for high performance applications [1,2]. Despite this limitation, PEK has been studied for electrical, optical, and filtration applications [3–8]. Thin films processed from polyphosphoric acid (PPA) doped PEK have been studied for their opto-electronic as well as anti-piezoelectric effects [4,7,8]. Chemically modified PEK membranes exhibit both good selectivity and permeation flux for gases and liquids in ultra-filtration applications [3,5,6]. PEK hollow fibers have also been processed to be used for gas filtration applications [9]. More recently, poly(ether ether ketone) (PEEK)/carbon nanotube bulk composites are also processed, showing improved thermal stability and mechanical properties [3,10–14].

In this study, *in-situ* polymerization was used to graft PEK onto few wall carbon nanotube (FWNT) [15–17]. Using this approach, fibers with PEK/FWNT weight ratio in the range of 99/1 to 80/20, have been processed. The resulting composite fibers were characterized for their structure, mechanical and thermomechanical properties, and electrical conductivity. These fibers exhibit exceptional toughness and good electrical conductivity, coupled with good thermal stability – thermal degradation onset temperature of above 500 °C.

2. Experimental

2.1. Materials

All reagents and solvents were purchased from Sigma–Aldrich, Co. and used as received, unless otherwise mentioned. The monomer, 4-phenoxybenzoic acid (4-PBA), was purified by recrystallization from toluene/heptanes to give shiny colorless

* Corresponding author. Interdisciplinary School of Green Energy/Institute of Advanced Materials & Devices, Ulsan National Institute of Science and Technology, Ulsan, 689-798, South Korea. Tel.: +82 52 708 7034; fax: + 82 52 708 7010.
** Corresponding authors.
E-mail addresses: hangi.chae@gatech.edu (H.G. Chae), satish.kumar@ptfe.gatech.edu (S. Kumar), jbbaek@unist.ac.kr (J.-B. Baek).
[1] Current address: PTD Group, Intel Corporation, Hillsboro, OR 97124, USA.
[2] Current address: Department of Mechanical and Industrial Engineering, Northeastern University, Boston, MA 02115, USA.

0032-3861/$ – see front matter © 2010 Elsevier Ltd. All rights reserved.
doi:10.1016/j.polymer.2010.06.034

Table 1
Feed ratios of monomer and FWNT, and solid contents for various PEK-g-FWNT solutions.

FWNT content (wt%)	Monomer + FWNT (g)	PPA (g)	P_2O_5 (g)	Solid content (wt%)
0	5.0 + 0	50	12.5	7.3
1	4.95 + 0.05	50	12.5	7.3
5	4.75 + 0.25	50	12.5	7.3
10	4.50 + 0.50	50	12.5	7.3
20	4.00 + 1.00	50	12.5	7.3

needles (m.p. 162–164 °C). Few wall carbon nanotube (FWNT, XO437VA, 4 wt% catalytic impurity) were obtained from Unidym, Inc. (Houston, TX) [18].

2.2. In-situ polymerization of 4-PBA in the presence of FWNT

For PEK and PEK-g-FWNT synthesis, a 250 mL flask equipped with a high torque mechanical stirrer, nitrogen inlet and outlet, and a solid-addition port was used. For 1% FWNT containing PEK-g-FWNT, 4-PBA (4.95 g, 23.1 mmol), FWNT (0.05 g), P_2O_5 (25.0 g), and poly(phosphoric acid) (PPA, 100 g; 83% P_2O_5 assay) were mixed under dry nitrogen purge at 130 °C for 72 h. The resultant material was named as PEK-g-1%FWNT. As the reaction progressed at the polymerization temperature, the dope stuck to the stirring rod at 130 °C within 72 h and could not be efficiently mixed further. The same procedure was used to synthesize the PEK-g-FWNT with other FWNT concentrations (5, 10 and 20 wt%). The different solid content and feed ratios are listed in Table 1. The representative procedure of "direct" Friedel-Crafts acylation reaction in a mild reaction medium of PPA with additional phosphorous pentoxide (P_2O_5) has been described elsewhere [15]. Table 2 lists the calculated total number of grafting sites and degree of polymerization for PEK grafted onto FWNT. The assumptions for detailed calculation have been reported elsewhere [15–17,19]. The calculation procedure is as follows.

$$\text{PBA in product(wt\%)} = \frac{4 - \text{PBA in feed(wt\%)} \times 196.2(\text{FW } C_{13}H_8O_2)}{214.2(\text{FW } C_{13}H_{10}O_3)} \quad (1)$$

$$\text{FWNT in product(wt\%)} = 1 - \text{PBA in product(wt\%)} \quad (2)$$

$$\text{FWNT(mol)} = \frac{\text{FWNT in product(wt\%)}}{12.01} \quad (3)$$

$$\text{PEK(mol)} = \frac{\text{PEK in product(wt\%)}}{196.2} \quad (4)$$

Assuming that there are 2.35 arylcarbonylation sites for every 100 carbons of the FWNT [19],

$$\text{grafting site(mol)} = \text{FWNT(mol)} \times 0.0235 \quad (5)$$

$$\frac{\text{PEK DP}}{\text{chain}} = \frac{\text{PEK(mol)}}{\text{grafting site(mol)}} \quad (6)$$

$$\frac{\text{PEK MW}}{\text{chain}} = \frac{\text{PEK DP}}{\text{chain}} \times 196.2 \quad (7)$$

During *in-situ* grafting polymerization of PEK, the number of grafting sites increases with increasing CNT concentration. Thus the molecular weight of the grafted chain decreases. As listed in Table 2, it should be noted that the calculated molecular weight of grafted PEK with 10 wt% FWNT is expected to be 10 times lower than that of grafted PEK with 1 wt% FWNT.

2.3. Fiber spinning

The fibers were spun by dry-jet wet-spinning using the small scale spinning system manufactured by Bradford University Research, Ltd (UK). The PEK-g-FWNT/PPA solution was placed into barrel (28 mm internal diameter). The solution was extruded through a single-hole spinneret of 120 μm diameter equipped with filter (mesh size was 20 μm) and passed through distilled water coagulation bath (~1.2 m long) maintained at room temperature. The as-spun fiber was kept immersed in water for several days to remove the residual PPA and the bath water was periodically replaced with fresh water. The fibers were subsequently drawn at various draw ratios at 200 °C. The different draw ratio is due to the different drawability of various fibers, and the draw ratio obtained in this study was the highest draw ratio achievable for each fiber. Fig. 1 shows the PEK and PEK-g-FWNT fibers on spools.

2.4. Fiber characterization

The tensile properties were measured using RSA III solid analyzer (TA Instruments). A gauge length of 25 mm was used for tensile, and 10–20 single filaments were tested for each sample at a strain rate of 1%/s. Wide-angle X-ray diffraction (WAXD) was performed on a multi-filament bundles of fiber using a Micro-Max002 X-ray source (Ni filtered CuKα, operating voltage and current at 45 kV and 0.66 mA, respectively, λ = 0.15418 nm) equipped with an *R*-axis IV++ 2D detection system (Rigaku/MSC Corp.). WAXD diffraction patterns/data were analyzed using the software packages of AreaMax V.1.00 and MDI Jade 6.1. The Raman spectra were collected using Witek (Alpha 300R) confocal Raman microscope with Nikon 20× objective lens (NA = 0.4) in back scattering configuration. The excitation laser wavelength was 514 nm. The dynamic mechanical properties of fibers were measured using thermomechanical analyzer (TMA, Q400, TA Instruments, Co.). For dynamic mechanical properties, temperature sweep test was conducted on a single filament in the temperature range of −50 to 300 °C at a constant heating rate of 1 °C/min. The pretension and stress amplitude for dynamic mechanical analysis were 15 and 3 MPa, respectively. The dimensional stability of fibers

Table 2
Calculated total number of grafting sites, degree of polymerization, and molecular weight of PEK grafted onto FWNT.

FWNT in feed (wt%)	4-PBA in feed (wt%)	PEK in product (wt%)	FWNT in product (wt%)	FWNT (mol)	PEK (mol)	Grafting site (mol)	PEK DP/chain	PEK MW/chain (g/mol)
0	100	100.0	0.0	0.00	0.51	N/A	N/A	N/A
1	99	98.9	1.1	0.09	0.50	0.0021	236.2	46,344
5	95	94.6	5.4	0.45	0.48	0.0106	45.3	8894
10	90	89.2	10.8	0.90	0.45	0.0212	21.5	4213
20	80	78.6	21.4	1.79	0.40	0.0420	9.5	1872

Fig. 1. Photograph of PEK and various PEK-g-FWNT fibers. The numbers on fiber spool represent the FWNT concentration.

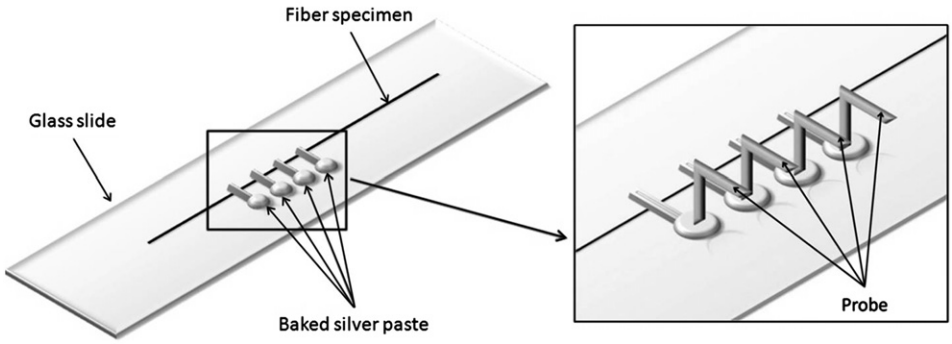

Fig. 2. The schematic description of electrical conductivity measurement setup.

(shrinkage behavior) was monitored on a single filament using a TMA at a constant heating rate of 10 °C/min in nitrogen using 1 MPa pretension. The thermal stability and char yield in nitrogen was measured using thermogravimetric analyzer (TGA, Q5000 by TA Instruments, Co.). Scanning electron microscope (SEM, LEO 1530, operated at 10 kV) was used for micro-structural analysis. For obtaining cross-sectional images, fiber thin-sections were prepared using embedding materials (electron microscopy sciences, Cat. # 14310). The axial direct current (DC) electrical conductivity of the composite fibers was measured using four point probe (Signatone, Co.) coupled with Keithley 2400 sourcemeter. The schematic description for conductivity measurement is given in Fig. 2. High-resolution transmission electron microscopy (HR-TEM) was performed on HF2000 TEM microscope (operated at 200 kV) and a JEOL 4000EX TEM microscope (operated at 400 kV). Charred fiber samples were grounded into fine powder using a mortar and pestle, and this powder was placed on Lacey carbon coated 300 mesh copper TEM grids (electron microscopy sciences, Cat. # LC325-Cu) for HR-TEM observation.

3. Results and discussion

Fig. 3 shows the cross-sectional SEM images of PEK and various PEK-g-FWNT composite fibers. It can be noted that PEK-g-20% FWNT fiber shows highly porous structure while the other fibers appear to have relatively solid cross-sectional structure. Based on the cross-sectional images, average fiber diameter was obtained and used for tensile testing. Tensile testing results are listed in Table 3. Draw ratios of each specimen are also listed in Table 3.

Fig. 4 shows the typical stress–strain curves of PEK and various PEK-g-FWNT composite fibers. Control PEK fibers have the highest tensile strength as compared to those of PEK-g-FWNT composite fibers, whereas PEK-g-20%FWNT fibers have the highest tensile modulus (~17 GPa). The low tensile strength in composite fibers may be attributed to the low molecular weight PEK as shown in Table 2, and the high modulus in PEK-g-20%FWNT fiber would be due to the large contribution from FWNT. Among various heat-drawn PEK and PEK-g-FWNT fibers, the 5% FWNT containing fiber showed the highest strain to failure of about 53%, resulting in toughness of about 122 J/g. The as-spun control PEK fibers exhibited very high toughness values, up to ~130 J/g. By comparison, the toughness values for high performance commercial fibers such as Kevlar™ (~30–45 J/g) and Zylon™ (~50 J/g) are significantly lower [20,21], while the toughness for spider silk is higher (about 170 J/g) [22].

The axial direct current (DC) electrical conductivity data of various PEK-g-FWNT fibers are listed in Table 3. At 5% FWNT loading, electrical conductivity was 2×10^{-4} S/m and this increased to 25 and 240 S/m, at 10 and 20 wt% FWNT loading, respectively. A five order magnitude increase in electrical conductivity with increasing FWNT concentration from 5 to 10% suggests that percolation threshold for FWNT in these oriented PEK-g-FWNT fibers is between 5 and 10 wt%.

2D WAXD patterns, integrated and equatorial scans of PEK and PEK-g-FWNT fibers are shown in Fig. 5. Based on WAXD studies of PEK [23], the crystallographic reflections are indexed based on an orthorhombic unit cell with lattice parameters $a = 0.763$ nm, $b = 0.596$ nm, and $c = 1.0$ nm. In this work, PEK orientation in the fibers was determined from WAXD data, where the Herman's orientation factor, f_c was determined by Wilchinsky's equation (Equations (8) and (9)) [24] using the (110) and (200) crystallographic planes.

$$\overline{\left(\cos\theta_{c-\mathrm{axis}}\right)^2} = 1 - \frac{\left(1-2\sin\rho_2^2\right)\left(\overline{\cos\varphi_1}\right)^2 - \left(1-2\sin\rho_1^2\right)\left(\overline{\cos\varphi_2}\right)^2}{\sin\rho_1^2 - \sin\rho_2^2} \tag{8}$$

$$f_c = \frac{3\left(\overline{\cos\theta_{c-\mathrm{axis}}^2}\right) - 1}{2} \tag{9}$$

The subscripts, 1 and 2 represent the two *hkl* planes, (110) and (200), used in the orientation characterization, and ρ is the angle between the given plane normal and the *a*- or *b*-axis. Thus, ρ values for (110) and (200) are calculated with respect to the *b*-axis to be ~52° and 0°, respectively. The (110) and (200) azimuthal intensity was used to calculate $(\cos\varphi)^2$ for the two planes. Using this approach $\overline{(\cos\theta_{c-\mathrm{axis}})^2}$ and f_c for the PEK and PEK/FWNT fibers was

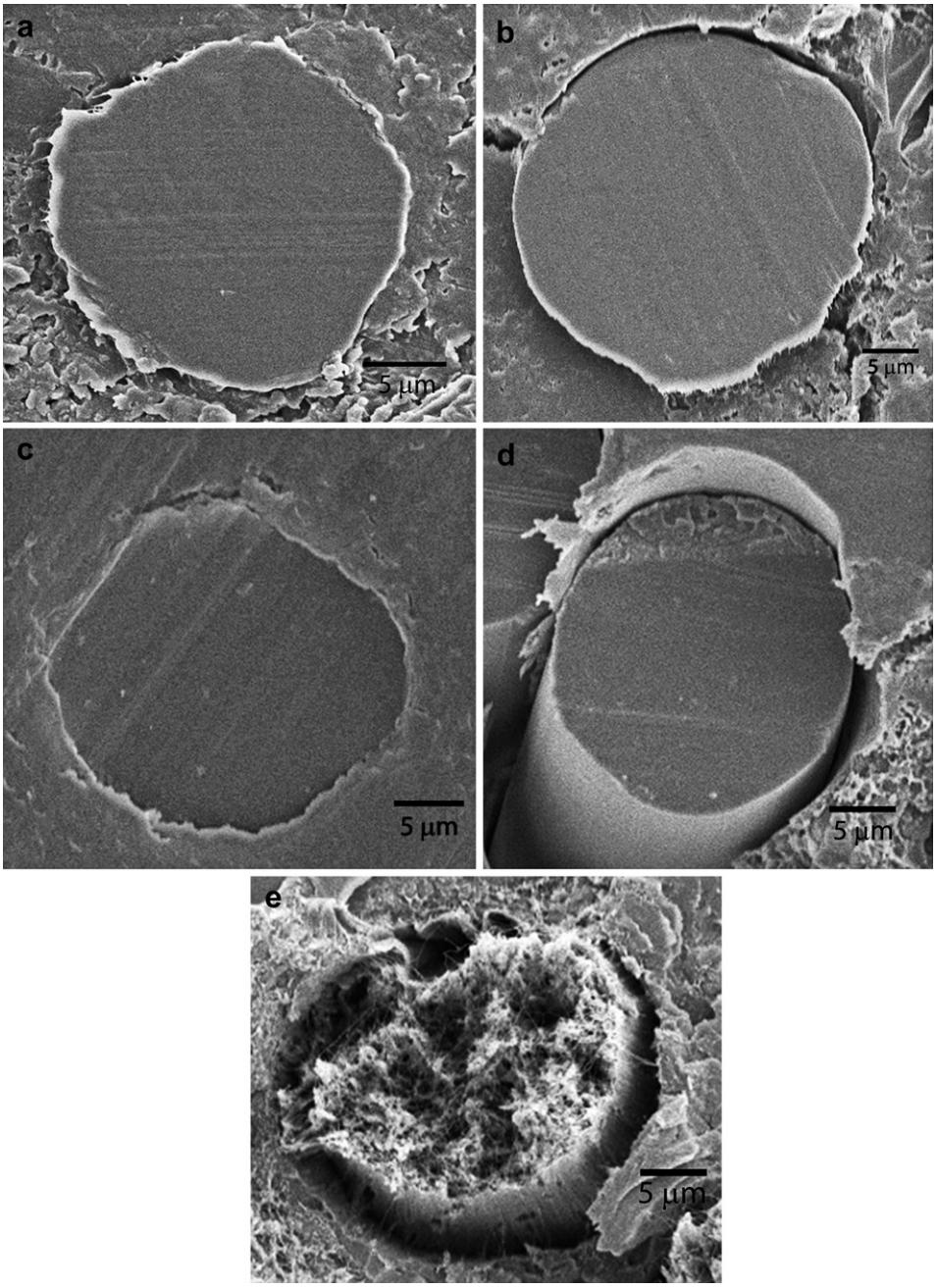

Fig. 3. Cross-sectional SEM images of (a) PEK, (b) PEK-g-1%FWNT, (c) PEK-g-5%FWNT, (d) PEK-g-10%FWNT, and (e) PEK-g-20%FWNT fibers.

Table 3
Mechanical properties and DC electrical conductivity of PEK and various PEK-g-FWNT fibers.

FWNT content (%)	Draw ratio	Fiber diameter (μm)	Tensile strength (MPa)	Tensile modulus (GPa)	Strain to failure (%)	Toughness[a] (J/g)	Electrical conductivity (S/m)
0	As-spun	32.6	130 ± 10	3.8 ± 0.1	163 ± 37	130 ± 37	N/A
0	2.3	21.1 ± 1.5	486 ± 12	10.6 ± 0.3	30 ± 4	90 ± 18	N/A
1	2.7	25.4 ± 2.4	297 ± 7	6.6 ± 0.3	30 ± 4	55 ± 8	N/A
5	As-spun	36.2	131 ± 10	4.9 ± 0.4	137 ± 19	109 ± 23	N/A
5	2.3	22.3 ± 1.2	359 ± 11	9.4 ± 0.7	53 ± 8	122 ± 23	$2.1 \times 10^{-4} \pm 5.9 \times 10^{-6}$
10	3.7	23.9 ± 0.4	191 ± 6	7.2 ± 0.5	18 ± 3	21 ± 5	25 ± 7
20	1.1	24.9 ± 1.4	122 ± 11	17.3 ± 1.3	3 ± 1	2 ± 1	240 ± 88

[a] Toughness was calculated from the area under the stress–strain curve.

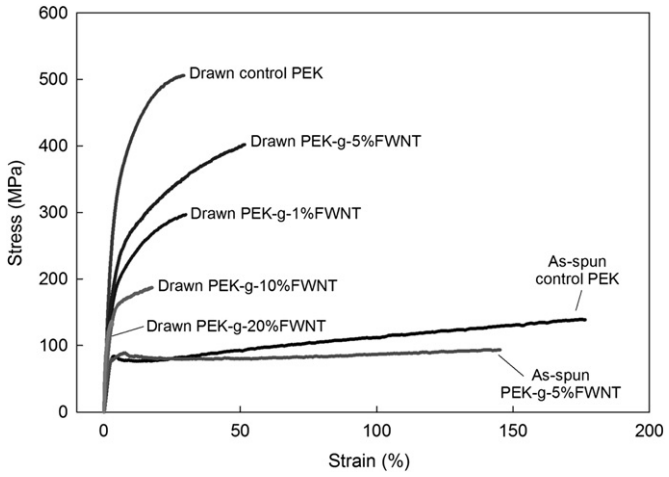

Fig. 4. Typical stress–strain curves of PEK and various PEK-g-FWNT composite fibers.

calculated and these values are listed in Table 4. The experimentally determined Herman's orientation factors of the fibers show a decreasing trend as the loading of FWNT is increased. PEK orientation is quite low (orientation factor less than 0.45). The overall drawability of the fibers decreased with increasing nanotube loading, which is related to low molecular weight of grafted PEK at high FWNT concentration. Low draw ratio results in reduced PEK orientation. Additionally, the crystallinity and crystal size of PEK exhibited similar trend as PEK orientation (Table 4).

For determining FWNT orientation, one can use WAXD diffraction, but the intensity from FWNT for most of the fibers was not distinguishable as shown in Fig. 5 because of intensity overlap by PEK crystal reflection. Therefore, the FWNT orientation in PEK-g-FWNT fibers was evaluated from the Raman spectroscopy. It is well known that the Raman G-band intensity decreases as increasing the angle between the CNT axis and the polarization direction of the incident laser [25]. Fig. 6a shows the G-band intensity variation of PEK-g-20%FWNT fiber when the fiber was placed with an angle of 0, 30, 60, and 90° to the incident laser polarization direction. As discussed, the G-band intensity exhibits the angular dependence. By comparing the G-band intensity ratio when the fiber is parallel (I_0) to the polarization direction of incident light and when it is perpendicular (I_{90}), one can estimate how well CNTs are aligned along the fiber axis. The higher the I_0/I_{90} ratio, higher is the degree of FWNT alignment in fiber axis direction. At 1% loading, meaningful Raman intensity could not be observed in these fibers due to the intensity overlap by fluorescence from PEK. For PEK-g-5%FWNT, PEK-g-10%FWNT, and PEK-g-20%FWNT fibers, the experimental I_0/I_{90} ratios were ~2.9, 3.7, and 4.3 respectively. It is reported that highly drawn polymer/CNT composite fibers often exhibited G-band I_0/I_{90} ratio greater than 40 [26,27], indicating that the FWNT orientation obtained in this study is relatively low. Thus, we observe that orientation of both the carbon nanotubes as well as PEK molecules is relatively low in these fibers. The Raman spectrum for pristine FWNT is also given in Fig. 6b.

Fig. 7 shows the dynamic mechanical properties of PEK and various PEK-g-FWNT composite fibers. PEK-g-20%FWNT composite fiber exhibits significantly different relaxation behavior as compared to the other fibers (Fig. 7a). In addition, control PEK and PEK-g-1%FWNT fibers have comparable trend, and PEK-g-5%FWNT and PEK-g-10%FWNT fibers show similar relaxation behavior. The absolute storage modulus at room temperature exhibited similar trend as compared to the tensile modulus of various fibers as listed in Table 3. The glass transition temperature for both PEK and PEK-g-1%FWNT fibers (measured from the tan δ peak position) was around 210 °C (Fig. 7b), while that of PEK-g-20%FWNT is about 190 °C. For comparison, much lower value of glass transition temperature (around 150–165 °C) have been reported in the

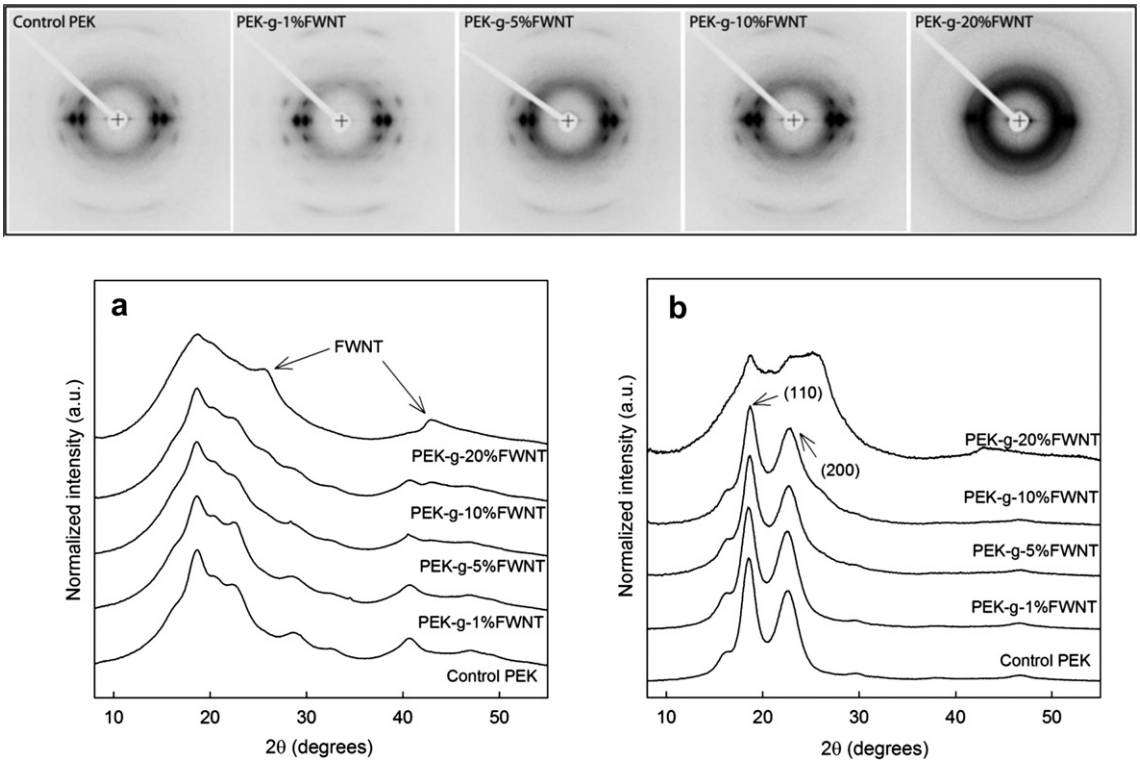

Fig. 5. Wide-angle X-ray diffraction (WAXD) patterns of PEK and PEK-g-FWNT composite fibers. (a) Integrated and (b) equatorial scans of WAXD patterns. The integrated and equatorial intensity profiles of composite fibers were shifted upward for clear comparison.

Table 4
WAXD analysis results of drawn PEK and various drawn PEK-g-FWNT fibers.

	Draw ratio	Crystallinity (%)	$\overline{(\cos\theta_{c-\text{axis}})^2}$	f_c (PEK)[a]	Crystal size (nm)[b]	
					$(110)_{2\theta\sim18.5^\circ}$	$(200)_{2\theta\sim22.5^\circ}$
PEK	2.3	48	0.66	0.49	4.8	3.3
PEK-g-1%FWNT	2.7	45	0.63	0.44	4.8	3.3
PEK-g-5%FWNT	2.3	35	0.61	0.41	4.7	3.2
PEK-g-10%FWNT	3.7	35	0.60	0.40	4.1	3.0
PEK-g-20%FWNT	1.1	27	0.40	0.10	3.8	2.5

[a] PEK crystal orientation was calculated based on Wilchinsky's equation as described in text.
[b] Crystal size was calculated based on equatorial scans using Scherrer's equation.

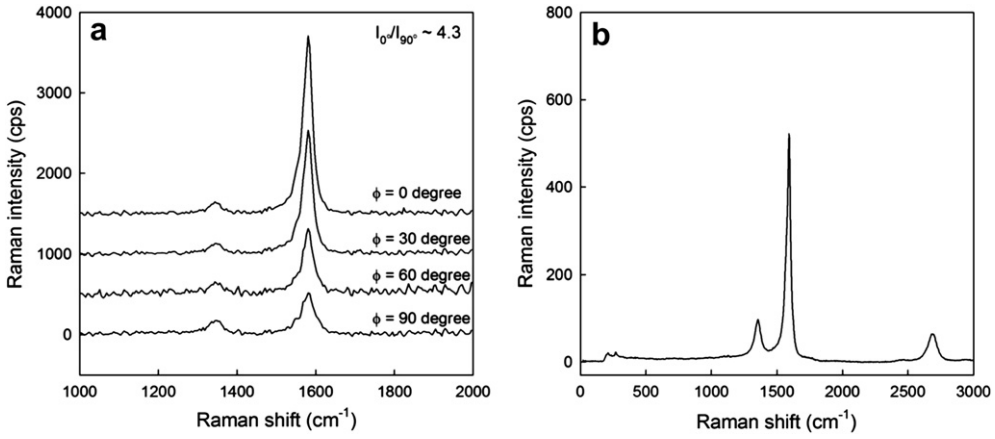

Fig. 6. (a) Raman G-band intensity variation of PEK-g-20%FWNT composite fiber as a function of angle between fiber and laser polarization direction in VV mode and (b) Raman spectrum of pristine FWNT. The spectra for 0, 30, and 60° in (a) were shifted upward for clear comparison. The VV mode represents that the direction of polarizer is parallel to the direction of analyzer, and 0° represents that the fiber axis direction is parallel to the polarizing direction. The intensity ratio of G-band (~1590 cm^{-1}) to D-band (~1300 cm^{-1}) of pristine FWNT was about 6.

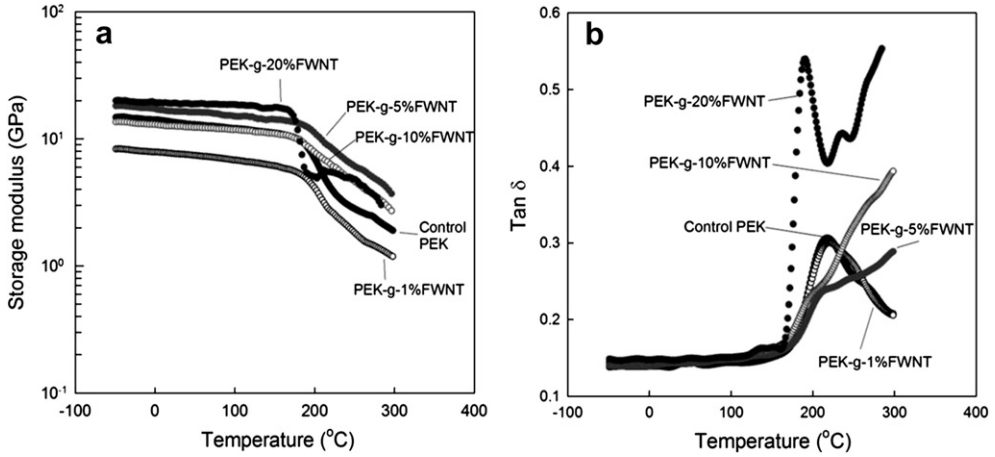

Fig. 7. Dynamic mechanical properties of drawn PEK and various drawn PEK-g-FWNT composite fibers. (a) Storage modulus and (b) tan δ behavior as a function of temperature. PEK-g-20%FWNT composite fiber exhibits significantly different relaxation behavior as compared to the other fibers. It shows very large amplitude of loss factor, which may be attributed to the low molecular weight of grafted PEK. For PEK-g-5%FWNT and PEK-g-10%FWNT fibers, tan δ peak is barely seen and the amplitude is weaker than those of control PEK and PEK-g-1%FWNT fibers.

Table 5
Coefficient of thermal expansion (CTE) of PEK and various PEK-g-FWNT fibers up to 150 °C in nitrogen.

	Draw ratio	CTE (/°C)
PEK	2.3	-2.82×10^{-6}
PEK-g-1%FWNT	2.7	-6.18×10^{-6}
PEK-g-5%FWNT	2.3	-4.51×10^{-6}
PEK-g-10%FWNT	3.7	-4.51×10^{-6}
PEK-g-20%FWNT	1.1	-8.44×10^{-6}

literature for the bulk PEK [23,28,29]. For PEK-g-5%FWNT and PEK-g-10%FWNT fibers, tan δ peak is barely seen and the peak amplitude is lower than that of control PEK and PEK-g-1%FWNT fibers. Furthermore, tan δ amplitude of PEK-g-5%FWNT and PEK-g-10% FWNT fibers continue to increase even above 210 °C (Fig. 7b). Similar tan δ behavior was observed for PAN/SWNT at 10 wt% SWNT [26,30] where polymer was not grafted on to CNT. The very large loss factor amplitude of PEK-g-20%FWNT fiber as compared to the other fibers may be attributed to the low molecular weight of grafted PEK. PEK and PEK-g-FWNT fibers showed good storage modulus retention even above glass transition temperature

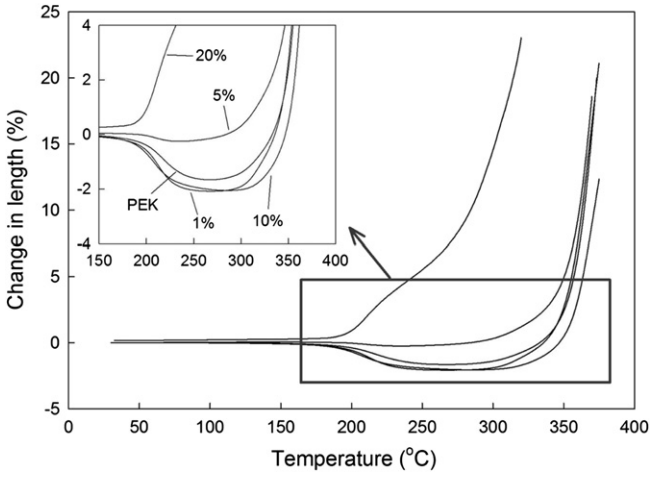

Fig. 8. Shrinkage behavior of PEK and PEK-g-FWNT composite fibers under nitrogen. Pretension and heating rate were about 1 MPa and 10 °C/min, respectively. Inset is the magnified behavior in boxed region for clear comparison. The numbers in inset represent the FWNT concentration.

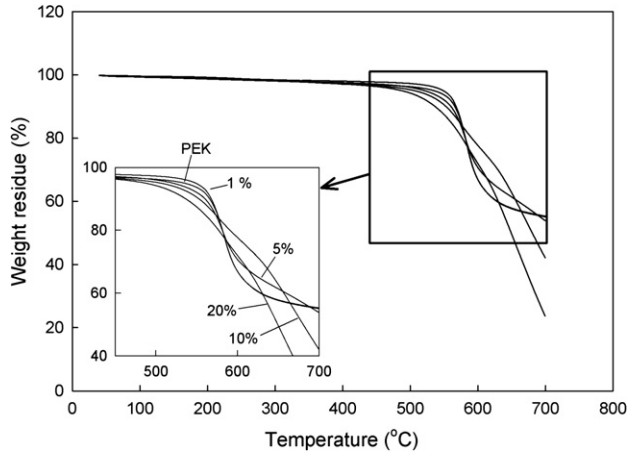

Fig. 9. TGA curves (in nitrogen at a heating rate of 10 °C/min) of PEK and PEK-g-FWNT composite fibers. Inset is the magnified weight loss behavior in boxed region for clear comparison. The numbers in inset represent the FWNT concentration.

(Fig. 7a) and its absolute value even at 300 °C was above 1 GPa for most fibers and above 3 GPa for 5, 10, and 20 wt% FWNT containing fibers. For comparison, poly(methyl methacrylate) showed more than two orders of magnitude decrease in storage modulus at glass transition and an absolute storage modulus of less than 0.1 GPa at just 130 °C [31]. In case of poly(ethylene terephthalate)/CNF composite fiber, storage modulus decreases to about 1 GPa at about 250 °C and would decrease to much below 1 GPa due to crystal melting (at higher than 265 °C) [32].

The thermal shrinkage behavior of PEK and PEK-g-FWNT fibers was studied in N_2 atmosphere. The fibers showed almost no shrinkage up to 150 °C. CTE data in the temperature range of room temperature to 150 °C is between −2 and −9 parts per million per °C (Table 5), and the shrinkage up to 300 °C was less than 2% (Fig. 8). As expected fibers showed significant expansion in the vicinity of melting point of PEK (300–350 °C). The PEK-g-5%FWNT fiber showed the best dimensional stability (less than 0.5% shrinkage) up to 300 °C and the coefficient of thermal expansion (CTE) in the range of 180–250 °C was $\sim -1.2 \times 10^{-5}$/°C. The PEK-g-20%FWNT fiber showed almost no shrinkage or expansion up to 190 °C, and abrupt expansion at above 190 °C. This behavior can be confirmed by WAXD analysis results, showing that this sample has very low degree of crystallinity and relatively small crystal size. This also could be due to the fact that PEK-g-20%FWNT fiber had lower draw ratio (DR ~1.1) and consequently low or no entropic thermal shrinkage. As discussed earlier, since the grafting sites increase with increasing FWNT concentration, the molecular weight of each grafted chain decrease with increasing FWNT concentration. Consequently, the polymer chain entanglement is expected to be reduced. Thus, in the PEK-g-20%FWNT, the polymer chain entanglements would be significantly lower than the other fibers.

Thermal stability of PEK and various PEK-g-FWNT fibers in inert environment is shown in Fig. 9. Up to 5 wt% FWNT loading, the composite fibers showed comparable degradation behavior as the control PEK fiber (~55 wt% char yield at 700 °C). However, at higher FWNT loadings of 10 and 20 wt%, the char yield at 700 °C in nitrogen reduced to 42 and 24 wt%, respectively. This indicates relatively low char yield of PEK in these fibers (32% and 4% for 10 and 20% CNT containing fibers, respectively, assuming the same weight loss for FWNT at 700 °C in inert environment [33]) as compared to that of the control PEK fiber (55%). The degradation of the polymer is dependent on the polymer molecular weight, and the thermal stability of the polymer decreases with increasing number of chain ends, i.e. with decreasing chain length. As

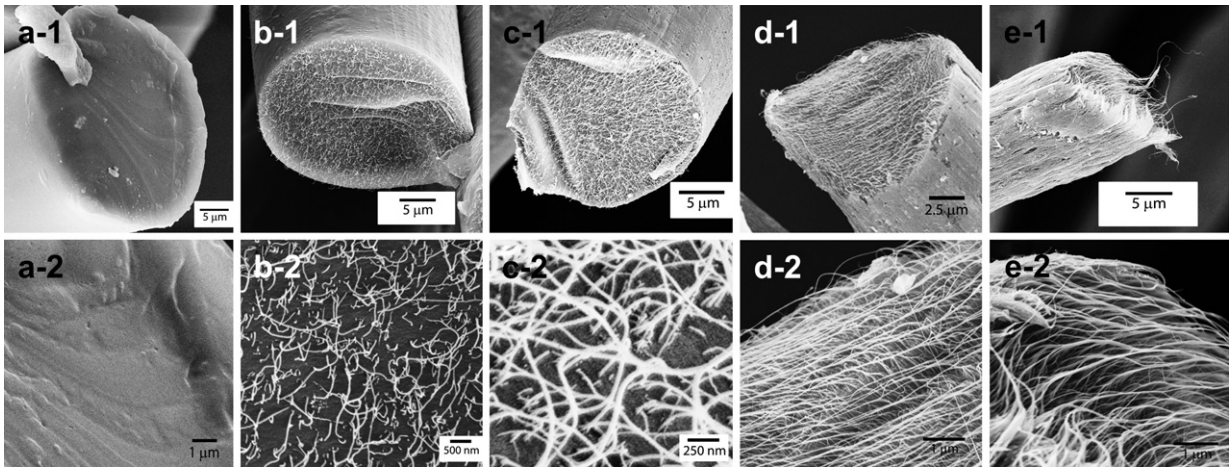

Fig. 10. SEM images of fractured surface of charred PEK and various PEK-g-FWNT composite fibers. (a) control PEK, (b) PEK-g-1%FWNT, (c) PEK-g-5%FWNT, (d) PEK-g-10%FWNT, and (e) PEK-g-20%FWNT.

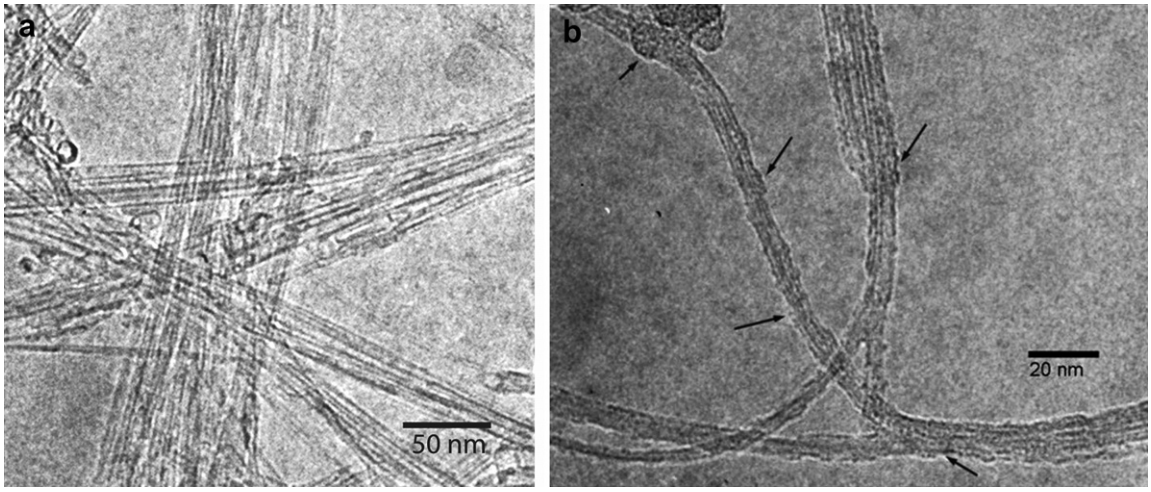

Fig. 11. High-resolution transmission electron micrograph of (a) pristine FWNT and (b) PEK/FWNT (1 wt% FWNT loading) fiber heat-treated at 700 °C showing charred PEK residue (arrows) from PEK grafted to FWNT. Charred fiber samples were grounded into fine powder using a mortar and pestle, and this powder was placed on Lacey carbon coated 300 mesh copper TEM grids (electron microscopy sciences, Cat. # LC325-Cu) for HR-TEM observation.

discussed earlier, the molecular weight of grafted PEK chain decreases with increasing FWNT concentration. Therefore, char yield of high FWNT concentration fibers decreased. The SEM images of the fibers treated at 700 °C in nitrogen are shown in Fig. 10. In all composite fiber cases, the FWNTs appear to be uniformly distributed in the fiber. The fracture surfaces also show that the FWNT containing fibrils are at least 10 μm long (Fig. 10e-2). Also the diameter of these fibrils is in the range of 30–40 nm, which is much larger than the original nanotube diameter of about 5 nm. High-resolution transmission electron micrographs (HR-TEM) studies on the charred fiber (PEK-g-1%FWNT) showed some amorphous material surrounding the surface of the FWNT (Fig. 11b). For comparison, the HR-TEM image of pristine FWNT is also given in Fig. 11a. Since PEK is grafted to FWNT, charred PEK during heat treatment remains coated on the FWNT.

4. Conclusions

The PEK and various PEK-g-FWNT fibers were successfully spun with FWNT concentration as high as 20 wt%. The FWNTs were found to be uniformly distributed and dispersed in the composite fibers. The control PEK and composite fibers possess high thermal stability with less than 5% weight loss up to 500 °C in nitrogen. With increasing FWNT concentration, crystallinity and crystal size of PEK decreased due to the high degree of grafting. The as-spun control PEK fiber showed very high toughness (up to 130 J/g), which surpassed many of the high performance fibers such as Kevlar™ and Zylon™. At 20 wt% FWNT loading, the fiber exhibited good electrical conductivity of 240 S/m. PEK and various PEK-g-FWNT composite fibers showed low degree of thermal shrinkage up to 150 °C. The 10 wt% FWNT containing fibers exhibited electrical conductivity of 25 S/m and toughness value of 21 J/g.

Acknowledgement

Financial support for this work from the National Science Foundation, Air Force Office of Scientific Research and World Class University (WCU) through the National Research Foundation (NRF) of Korea funded by the Ministry of Education, Science and Technology (MEST) are gratefully acknowledged.

References

[1] Fried JR. In: Mark JE, editor. Polymer data handbook. New York: Oxford University Press; 1999. p. 479.
[2] Teasley MF, Hsiao BS. Macromolecules 1996;29:6432;
Wood AS. Mod Plast Int 1987;88.
[3] Li LC, Wang BG, Tan HM, Chen TL, Xu JP. J Membr Sci 2006;269:84.
[4] Pan QW, Fang CS, Qin ZH, Gu QT, Cheng XF, Xu D, et al. Mater Lett 2003;57:2612.
[5] Qiu CQ, Nguyen QT, Ping ZH. J Membr Sci 2007;295:88.
[6] Qiu CQ, Xu F, Nguyen QT, Ping ZH. J Membr Sci 2005;255:107.
[7] Shi W, Fang CS, Pan QW, Sun X, Gu QT, Xu D, et al. J Mater Sci Lett 2000;19:147.
[8] Shi W, Yin X, Fang CS, Pan QW, Gu QT, Wu XW, et al. Opt Lasers Eng 2001;35:121.
[9] Ying S, Rogers-Gentile V, Brown PJ. J Text Inst 1999;90:30.
[10] Bangarusampath DS, Ruckdaschel H, Altstadt V, Sandler JKW, Garray D, Shaffer MSP. Polymer 2009;50:5803.
[11] Diez-Pascual AM, Naffakh M, Gomez MA, Marco C, Ellis G, Gonzalez-Dominguez JM, et al. Nanotechnology 2009;20:315707.
[12] Diez-Pascual AM, Naffakh M, Gomez MA, Marco C, Ellis G, Martinez MT, et al. Carbon 2009;47:3079.
[13] Li J, Zhang LQ. Proc Inst Mech Eng C Mech Eng Sci 2009;223:2501.
[14] Li J, Zhang LQ. Mech Compos Mater 2009;45:495.
[15] Baek JB, Lyons CB, Tan LS. J Mater Chem 2004;14:2052.
[16] Baek JB, Tan LS. Polymer 2003;44:4135.
[17] Baek JB, Lyons CB, Tan LS. Macromolecules 2004;37:8278.
[18] www.unidym.com.
[19] Wang DH, Tan L-S, Huang H, Dai L, Osawa E. Macromolecules 2009;42:114.
[20] Chae HG, Kumar S. In: International SAMPE symposium and exhibition, Long Beach, CA; 2005.
[21] Chae HG, Kumar S. J Appl Polym Sci 2006;100:791.
[22] Vollrath F, Knight DP. Nature 2001;410:541.
[23] Dawson PC, Blundell DJ. Polymer 1980;21:577.
[24] Wilchinsky ZW. J Appl Phys 1960;31:1969.
[25] Liu T, Kumar S. Chem Phys Lett 2003;378:257.
[26] Chae HG, Minus ML, Kumar S. Polymer 2006;47:3494.
[27] Minus ML, Chae HG, Kumar S. Macromol Chem Phys 2009;210:1799.
[28] Harris JE, Robeson LM. J Polym Sci Part B Polym Phys 1987;25:311.
[29] Waddon AJ, Hill MJ, Keller A, Blundell DJ. J Mater Sci 1987;22:1773.
[30] Sreekumar TV, Liu T, Min BG, Guo H, Kumar S, Hauge RH, et al. Adv Mater 2004;16:58.
[31] Zeng JJ, Saltysiak B, Johnson WS, Schiraldi DA, Kumar S. Compos B Eng 2004;35:173.
[32] Ma HM, Zeng JJ, Realff ML, Kumar S, Schiraldi DA. Compos Sci Technol 2003;63:1617.
[33] Chae HG, Sreekumar TV, Uchida T, Kumar S. Polymer 2005;46:10925.